



**HAL**  
open science

## Spontaneous formation of barium sulfate crystals at liquid-liquid interfaces

Nazanin Ghaheri, Benjamin J.J. Austen, Grégoire Herzog, Mark I. Ogden, Franca Jones, Damien W M Arrigan

► **To cite this version:**

Nazanin Ghaheri, Benjamin J.J. Austen, Grégoire Herzog, Mark I. Ogden, Franca Jones, et al.. Spontaneous formation of barium sulfate crystals at liquid-liquid interfaces. *CrystEngComm*, 2022, 24, pp.7793-7802. 10.1039/D2CE01102F . hal-03824942

**HAL Id: hal-03824942**

**<https://hal.univ-lorraine.fr/hal-03824942v1>**

Submitted on 23 Nov 2023

**HAL** is a multi-disciplinary open access archive for the deposit and dissemination of scientific research documents, whether they are published or not. The documents may come from teaching and research institutions in France or abroad, or from public or private research centers.

L'archive ouverte pluridisciplinaire **HAL**, est destinée au dépôt et à la diffusion de documents scientifiques de niveau recherche, publiés ou non, émanant des établissements d'enseignement et de recherche français ou étrangers, des laboratoires publics ou privés.

# Spontaneous formation of barium sulfate crystals at liquid-liquid interfaces

Nazanin Ghaheri<sup>1</sup>, Benjamin J. J. Austen<sup>1</sup>, Grégoire Herzog<sup>2\*</sup>, Mark I. Ogden<sup>1</sup>, Franca Jones<sup>1\*</sup>,  
Damien W. M. Arrigan<sup>1\*</sup>

<sup>1</sup>School of Molecular and Life Sciences, Curtin University, Perth, Western Australia 6845, Australia

<sup>2</sup>Université de Lorraine, CNRS, LCPME, F-54000 Nancy, France

\* d.arrigan@curtin.edu.au; f.jones@curtin.edu.au; gregoire.herzog@cnrs.fr

## Abstract

Crystallisation at or near interfaces plays an important role in many environmental, biological and industrial processes. In this study, crystallisation was investigated at the interface between two immiscible solutions undergoing spontaneous transfer of ions. Using barium sulfate ( $\text{BaSO}_4$ ) as a model system, crystallisation at the aqueous-organic interface was investigated in cases where barium ions were placed in either the aqueous phase or the organic phase, and the co-reactant sulfate in the adjoining phase, respectively. Formation of precipitated solids was found in both cases, resulting from the spontaneous transfer of ions from the organic phase to the aqueous phase where precipitation occurred. Characterisation of precipitated solids was performed by Raman spectroscopy, scanning electron microscopy (SEM), energy dispersive X-ray spectroscopy (EDS) and transmission electron microscopy (TEM), confirming the crystallisation of  $\text{BaSO}_4$  at or close to the interface. The influence of a neutral ionophore in the organic phase on spontaneous formation of  $\text{BaSO}_4$  was also studied, demonstrating the capability to impede the transfer of ions and hence the precipitation process. Overall, these results provide a proof-of-principle demonstration of the ability to form ionic crystalline materials by exploiting ion transfer processes at the interface between immiscible liquids.

## 1. Introduction

Crystallisation of solids from solution plays a critical role in many industrial processes, whether beneficial, such as for pharmaceutical manufacturing,<sup>1-3</sup> minerals recovery and water treatment,<sup>4</sup> or detrimental, for example in the deposition of inorganic scale within oil and gas production processes.<sup>5</sup> Nucleation and crystal growth is also important in biomedical fields. For example, the crystallisation of haemoglobin C and haemoglobin S reduces the flexibility of red blood cells and causes sickle cell anemia,<sup>7, 8</sup> while phase transformation of proteins in the retina leads to the formation of cataracts.<sup>9</sup>

Scale is defined as an undesirable crystallisation product which can have many unwanted consequences such as loss of production, loss of product purity, and maintenance issues.<sup>10-14</sup> Barium sulfate ( $\text{BaSO}_4$ ) is a well-characterised inorganic scale, known as both a synthetic and mineral (barite) compound with a rich morphology,<sup>15-17</sup> excellent physical properties and good chemical stability.<sup>18</sup> According to the group of Putnis,<sup>19</sup> crystallisation of  $\text{BaSO}_4$  occurs through a non-classical mechanism, whereby smaller particles grow through oriented attachment. Homogenous nucleation and growth of  $\text{BaSO}_4$  has been investigated by morphological and chemical structural analysis.<sup>20</sup> Prevention of  $\text{BaSO}_4$  scale formation from supersaturated solutions was achieved by different additives or inhibitors. In particular, polyphosphonates<sup>14, 21</sup> and polyelectrolytes<sup>22</sup> are popular classes of inhibitors due to their high efficiencies.

Although intentional crystallisation of  $\text{BaSO}_4$  is useful in some biomedical applications, such as imaging or radiation protection,<sup>23, 24</sup> its formation in oil production, either within rock pores or in pipelines, limits the speed and extent of oil recovery.<sup>25</sup> In this situation, crystallisation occurs within a heterogeneous system. Heterogeneous nucleation processes often are considered to be the most practically important problems in crystallisation science.<sup>26</sup> Furthermore barite crystallisation is often used as a model process for understanding of more complex scenarios.<sup>27</sup> Although homogeneous  $\text{BaSO}_4$  nucleation and growth has been extensively studied, few investigations have been reported on heterogeneous  $\text{BaSO}_4$  crystallisation. One example is the heterogeneous nucleation and growth of  $\text{BaSO}_4$  at organic/water interfaces based on self-assembled monolayers of thiolated hydrocarbons with different functional groups at the end of the hydrocarbon chain.<sup>28, 29</sup> In that study, investigations were undertaken into the impact of interfacial interactions on heterogeneous nucleation and growth processes to substrates with controlled hydrophobicity. In another example of  $\text{BaSO}_4$  crystallisation at aqueous-organic interfaces, crystallisation at water-chloroform interfaces modified by a film of fatty acid was studied.<sup>30, 31</sup> In this case the liquid-liquid interface was formed and modified by the fatty acid and then the  $\text{BaSO}_4$  crystals were formed with both reactants present in the aqueous phase. Despite reports of  $\text{BaSO}_4$  and other inorganic depositions based on precipitation when the reacting ions are in the same aqueous phase,<sup>28, 30, 32, 33</sup> formation of inorganic crystals at oil-water (liquid-liquid) interfaces with one of the reactants initially present in the adjoining immiscible phase remains relatively unknown. In one example, calcium sulfate hydrates were grown at liquid-liquid interfaces formed between hydrocarbon phases containing surfactant-stabilised calcium carbonate particles and aqueous sulfuric acid.<sup>34</sup>

The interface formed between two immiscible electrolyte solutions (ITIES),<sup>35</sup> comprised of aqueous and organic electrolyte phases of low mutual miscibilities, offers a defect-free, repairable surface for

nucleation and growth and is a basis to explore new behaviours. Selective cocrystallisation at the ITIES, for instance, was achieved recently by controlling chemically the polarisation of the interface.<sup>36</sup> It was found that the imposition of electrical potential differences at the ITIES enabled control over the formation of caffeine cocrystal polymorphs. The aim of the work reported here was to investigate crystallisation of an inorganic material at or near the ITIES under conditions where one of the reactants arrives by spontaneous ion transfer from the adjoining phase and to identify ways that such spontaneous crystallisation may be controlled. Barium sulfate was chosen as a model system as it is well-known and characterised,<sup>16, 27</sup> its crystallisation is understood and it does not have added complexity such as the formation of hydrates as does calcium sulfate crystallisation. It is also relatively straightforward to place either reactant into the organic phase. Ionophores<sup>37</sup> are available which are known to bind to barium,<sup>38</sup> which provides a means to control the transfer of barium cations to the aqueous phase. Moreover, BaSO<sub>4</sub> crystallisation at liquid-liquid interfaces with either reactant arriving from the adjoining phase has not been reported. To achieve our aims, Ba<sup>2+</sup> ions were placed in either the aqueous or the organic phase and brought into contact with an adjoining liquid phase containing SO<sub>4</sub><sup>2-</sup> (Schemes 1 and 2). The solids formed upon contact between these immiscible phases were characterised by various techniques, notably Raman spectroscopy, scanning electron microscopy (SEM), energy dispersive X-ray spectroscopy (EDS) and transmission electron microscopy (TEM) in order to identify and verify the formation of barium sulfate. The impact of added ionophore was also assessed, as a strategy to control the spontaneous crystallisation. Control of crystallisation at the ITIES opens new ways to study and understand interfacial growth processes important in biomedical<sup>39, 40</sup> (e.g. crystals in synovial fluids) and geological<sup>27</sup> (e.g. crystal growth within rock formations) fields where soft interfaces are omnipresent.

## 2. Experimental

### 2.1 Chemicals

All reagents were of analytical grade. 1,2-dichloroethane (DCE) (Merck, 99.5% G.C. Grade) was employed as the organic solvent in all experiments. Ultra-pure water (18.2 MΩ.cm resistivity) was obtained freshly from a Milli-Q system (Millipore). Barium chloride, lithium chloride, barium sulfate, sodium sulfate, bis(triphenylphosphoranylidene)ammonium chloride (BTPPACl, 98 %), potassium tetrakis(4-chlorophenyl)borate (KTPBCl, 98 %), tetrabutylammonium hydrogensulfate (TBuAHSO<sub>4</sub>, 97%), chlorotrimethylsilane (99%) and Calcium Ionophore IV were purchased from Sigma Aldrich Chemical Co., Australia. Bis(triphenylphosphoranylidene)ammonium tetrakis(4-chlorophenyl)borate (BTPPATPBCl) was synthesized according to published procedures,<sup>41, 42</sup> and used as supporting

electrolyte in the DCE phase. Barium tetrakis(4-chlorophenyl)borate ( $\text{Ba}(\text{TPBCl})_2$ ) was prepared according to the published procedure<sup>43</sup> and confirmed by EDS and CHN analyses (Fig. S1, Supplementary Information). Ferric chloride hexahydrate ( $\text{FeCl}_3 \cdot 6\text{H}_2\text{O}$ , 99% Fluka) was used to prepare silver/silver chloride electrodes from silver wire (purity 99.99%, Advent Research Materials).

## 2.2 Apparatus

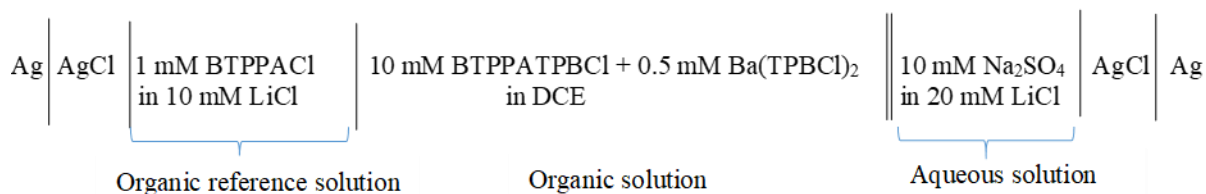
Two different experimental set-ups were used. The first involved a capillary glass tube to support the interface at its mouth and to visualise  $\text{BaSO}_4$  crystallisation at the interface. The second set-up was an electrochemical cell with a microporous array glass membrane so that interfaces were formed at the individual micropore mouths.

### 2.2.1 Glass capillary

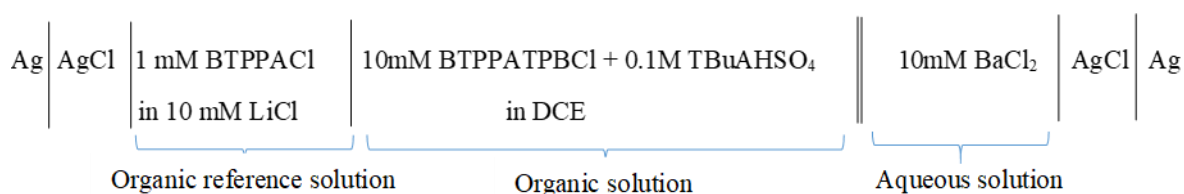
Precipitation of barium sulfate formed by spontaneous transfer of ions between two immiscible solutions was carried out in borosilicate glass capillaries having 0.58 mm inner diameter (ID), 1 mm outer diameter (OD) and 10 cm length (Sutter Instrument Co., USA). The inner walls of these capillaries were silanized with chlorotrimethylsilane (99%) to make them hydrophobic so that the inside was easily filled with the organic solution; the aqueous phase was placed outside the pipette (Figure 1(a)). The capillaries were filled from the back with organic solution using a 10  $\mu\text{L}$  syringe.

### 2.2.2 Microporous array glass membranes

Experiments were performed using a glass microporous array membrane, consisting of 100 ( $10 \times 10$  square array) pores in 130  $\mu\text{m}$  thick borosilicate glass substrates. The pores were formed by laser ablation.<sup>44</sup> The fabrication process produced conical pores, with a radius of 26.5  $\mu\text{m}$  at the laser entry side and a radius of 11.5  $\mu\text{m}$  at the laser exit side. The laser exit side of the glass membrane and the internal pore walls were functionalised with trichloro-(1*H*,1*H*,2*H*,2*H*-perfluorooctyl)silane to make them hydrophobic. All membrane fabrication and functionalisation took place at the Australian National Fabrication Facility. The hydrophobic side of the membrane was glued to a glass tube (~5.3 mm internal diameter) with silicone adhesive (Selley, Australia and New Zealand).<sup>45</sup> The silicone was allowed to cure for 24 h, and the assembled glass tube-membrane was rinsed with acetone/methanol and dried in air. The organic solution was placed into the tube-membrane assembly and then the organic reference solution was added on top. This assembly were then inserted into the aqueous phase and two Ag/AgCl electrodes (one in each phase) were inserted to enable electrochemical measurements (Schemes 1 and 2).



**Scheme 1.** Electrochemical cell composition used for investigating crystallisation following spontaneous barium ion transfer from organic to aqueous phase.



**Scheme 2.** Electrochemical cell composition used in investigating crystallisation following spontaneous transfer of hydrogen sulfate ions from organic to aqueous phase to form barium sulfate crystals.

## 2.3 Characterization

### *Raman Spectroscopy*

Confocal Raman spectra and optical images were collected at room temperature using a WITec alpha 300SAR, equipped with a frequency doubled NdYAG laser (wavelength 532 nm (green) or 633nm (red), power 50 mW). Each Raman spectrum consists of 100 accumulations at an integration time of 0.1 s and grating of 600 g/mm. Analysis was performed using WITec Project Four software.

### *Scanning electron microscopy (SEM) and Energy dispersive X-ray spectroscopy (EDS)*

The glass microporous array membrane on which crystals were formed was placed onto a double-sided carbon tape fixed to an SEM stub. The samples were then dried in a desiccator and coated with platinum (~4 nm) before analysing with a Tescan Mira3 SEM. Energy dispersive X-ray spectroscopy (EDS) was also employed to determine the elemental composition of samples. SEM-EDS results were processed using Oxford AZtec software to obtain information from selected particle areas.

### *Transmission Electron Microscopy (TEM)*

High resolution TEM (HRTEM), TEM, high angle annular dark field TEM (HAADF-TEM), elemental mapping images from EDS, and fast Fourier transform (FFT) patterns were obtained on a FEI Talos F200X FEG-TEM. To prepare the samples for TEM, after crystal growth, the glass membrane was sonicated in ethanol to remove precipitated particles from the membrane surface. This ethanol slurry was used to prepare a TEM grid with the particles.

### *Electrochemical measurements*

Open-circuit potential (OCP) experiments were conducted with an Autolab PGSTAT302N (Metrohm, The Netherlands) operated with the supplied NOVA software (Version 1.11). All measurements were performed at room temperature (22°C) with the glass membrane-based  $\mu$ ITIES array prepared as described above. Measurements of pH were made with a polypropylene bodied combination pH electrode (IJ-40A, Ionode, Australia) with an Elmetron CP-511 digital pH meter (Ionode, Australia).

## **3. Results and Discussion**

### **3.1 Interfacial barium sulfate crystallisation at a glass capillary**

Initially, the formation of BaSO<sub>4</sub> at the liquid–liquid interface was investigated visually by setting up an experiment at the interface located at the mouth of a glass capillary (Fig.1A). This would facilitate visual inspection of any insoluble reaction products as well as providing a basis for subsequent chemical characterisation. This experiment consisted of a glass capillary filled with an organic solution of 0.5 mM Ba(TPBCl)<sub>2</sub> and 10 mM BTPPATPBCl (background electrolyte) in DCE which was then inserted into a vial containing 10 mM aqueous Na<sub>2</sub>SO<sub>4</sub> solution. Dissolving Ba(TPBCl)<sub>2</sub> in DCE enables placement of Ba<sup>2+</sup> into the organic phase. Upon contact of this organic phase with an aqueous phase, spontaneous transfer of Ba<sup>2+</sup> ions to the aqueous phase is expected (Fig. 1B), due to the hydration energy (1305 kJ mol<sup>-1</sup>).<sup>46</sup> After standing overnight of the capillary containing Ba(TPBCl)<sub>2</sub> in DCE in an aqueous solution of Na<sub>2</sub>SO<sub>4</sub>, the formation of a new solid phase was observed at the capillary mouth. This is attributed to the spontaneous transfer of Ba<sup>2+</sup> cations across the interface where precipitation with SO<sub>4</sub><sup>2-</sup> occurred on the aqueous side of the interface. This experiment was repeated in ten glass capillaries and vials. Crystals formed at the liquid-liquid interface at the mouths of the capillaries were analysed by Raman spectroscopy. A typical Raman spectrum and optical microscope image of crystals are shown in Fig. 2. From the Raman spectra of many crystalline sulfates, four basic vibrational modes of SO<sub>4</sub> tetrahedra have been assigned:<sup>47, 48</sup>  $\nu_1$  is the strongest peak, near 1000 cm<sup>-1</sup>, attributable to the symmetric S–O stretching mode;  $\nu_2$  is assigned to the symmetric O–S–O bend modes near 460 cm<sup>-1</sup>;  $\nu_3$  is assigned to the asymmetric S–O stretch modes near 1100 cm<sup>-1</sup>; and  $\nu_4$  is assigned

to the asymmetric O–S–O bend modes near  $630\text{ cm}^{-1}$ . The Raman spectrum of the collected crystals (Fig. 2) shows all four vibrational modes of sulfate. Numerous relationships have been observed between the shift of the peak positions and the nature of the cations in the sulfates.<sup>48</sup> The most noticeable feature is that metal cations affect the disorder of sulfate solids formed.<sup>48, 49</sup> The lower symmetry due to the presence of a divalent metal cation in  $\text{BaSO}_4$  results in higher vibrational frequencies in sulfate's Raman spectrum and to the doublet at  $640\text{ cm}^{-1}$  (Fig. 2).<sup>49</sup>

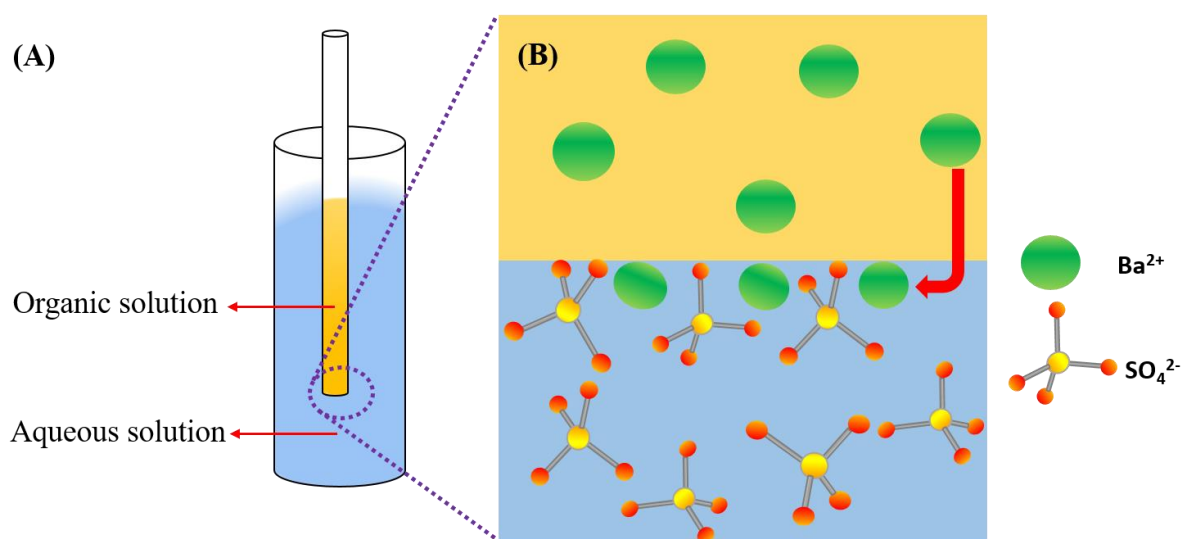


**Figure 1.**  $\text{BaSO}_4$  crystallisation at the liquid–liquid interface. (A) Schematic representation of the glass capillary experimental arrangement. The glass capillary contains  $0.5\text{ mM Ba(TPBCl)}_2$  and  $10\text{ mM BTPPATPBCl}$  (organic solution); the glass vial contains  $10\text{ mM Na}_2\text{SO}_4$  aqueous solution. (B) Schematic illustration of near-interface crystallisation via transfer of  $\text{Ba}^{2+}$  from the organic phase to the aqueous phase followed by  $\text{BaSO}_4$  precipitation at the capillary mouth.

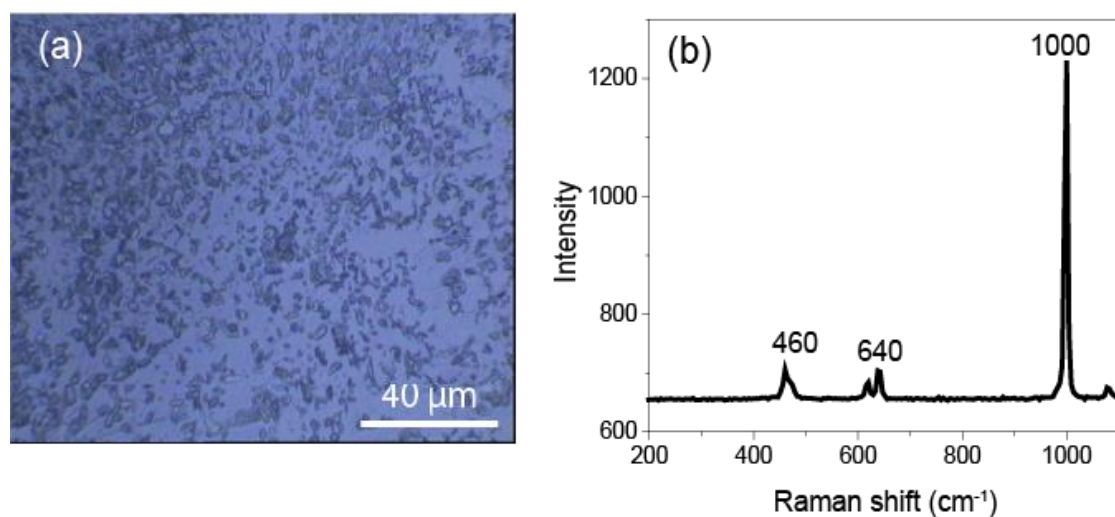


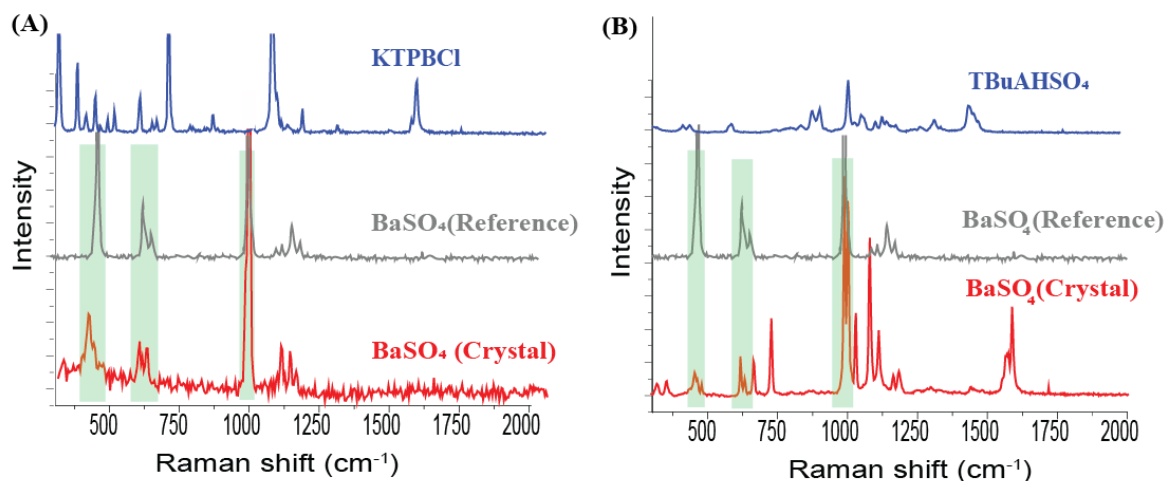


**Figure 2.** Confocal Raman microscopy and spectroscopic characterisation. (a) Optical image of BaSO<sub>4</sub> formed at the glass capillary mouth, (b) Raman spectrum of the observed crystals.

### 3.2 Crystal formation at interfaces formed in microporous glass membranes

Spontaneous formation of barium sulfate was also studied by using microporous arrays as supports for the liquid-liquid interface, forming arrays of microITIES. At such an array of microscale interfaces, the organic phase containing Ba<sup>2+</sup> (0.5 mM Ba(TPBCl)<sub>2</sub> and 10 mM BTPPATPBCl in DCE) was placed on one side of a microporous glass membrane and the aqueous solution of SO<sub>4</sub><sup>2-</sup> on the other (Scheme 1). The immiscible phases came in contact only at the mouths of the pores in the glass membrane.<sup>44</sup> The alternative arrangement with Ba<sup>2+</sup> in the aqueous solution and sulfate species in the organic phase (Scheme 2) was also studied. The Raman spectra in Fig. 3A show that barium sulfate deposition occurred at the interfaces formed between an organic phase containing Ba<sup>2+</sup> (i.e. 0.5 mM Ba(TPBCl)<sub>2</sub>) and an aqueous solution containing 10 mM Na<sub>2</sub>SO<sub>4</sub>. This is attributed to the transfer of Ba<sup>2+</sup> ions from the organic phase to the aqueous phase, driven by the large hydration energy,<sup>46</sup> where they reacted with sulfate anions and precipitated due to the low solubility of BaSO<sub>4</sub> (K<sub>sp</sub> = 10<sup>-10</sup>).<sup>50</sup>

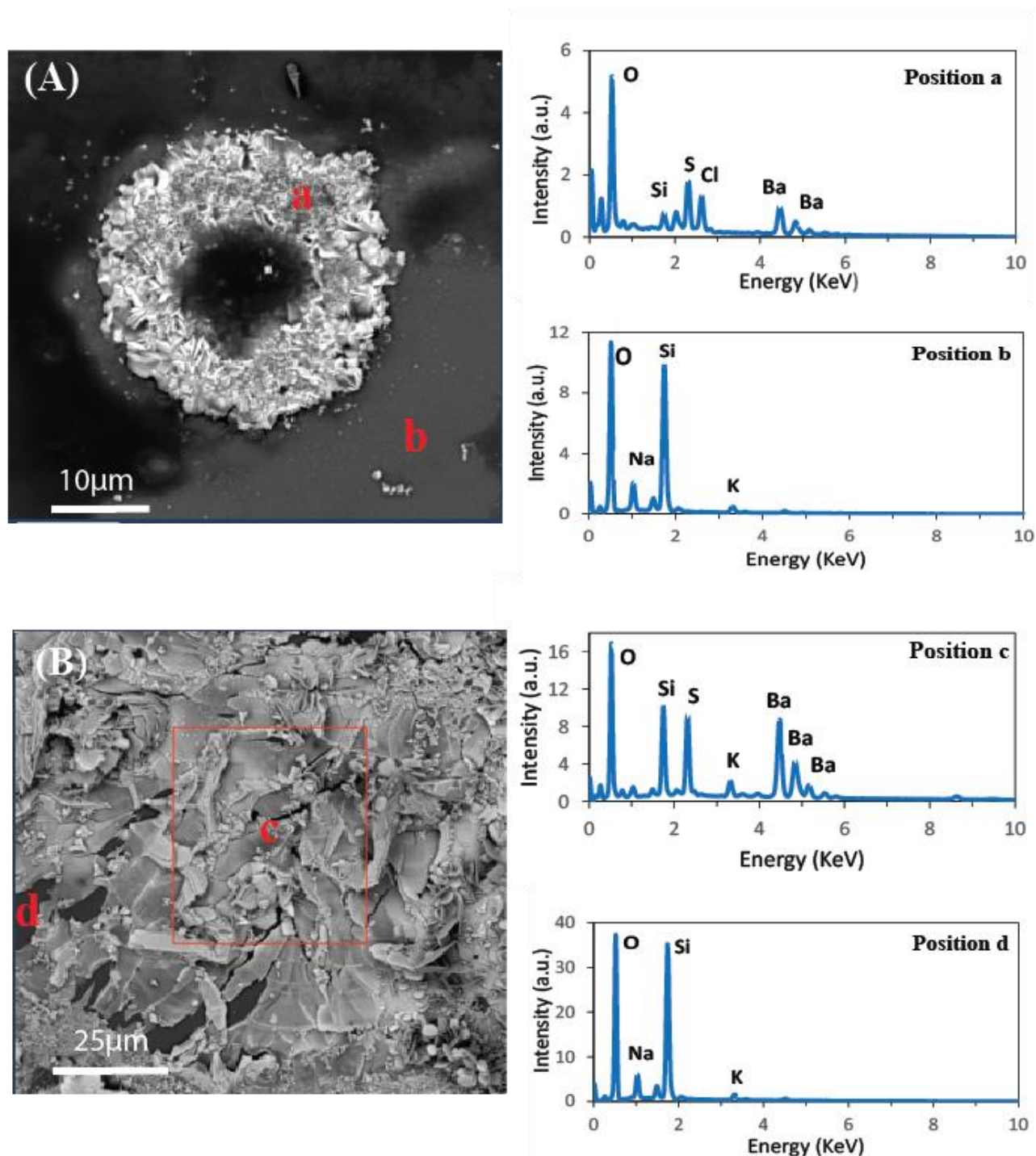
The formation of barium sulfate crystals at the aqueous side of the interface between an aqueous phase containing Ba<sup>2+</sup> and an organic phase containing TBuAHSO<sub>4</sub> (Scheme 2) is also supported by comparing the Raman spectra of the product formed with the spectra of commercially-sourced BaSO<sub>4</sub> and TBuAHSO<sub>4</sub> (Fig. 3B). These spectra show that the crystallisation product includes the most prominent peaks that are present in the reference BaSO<sub>4</sub> salt. The other peaks in the product spectra may be due to the other organic phase components. Additionally, the fate of protons resulting from the crystallisation when Ba<sup>2+</sup> (aqueous phase) and HSO<sub>4</sub><sup>-</sup> (transferred from the organic phase) came in contact was investigated by measuring the pH of the aqueous phase before and after the crystallisation experiments. Upon crystal formation, the pH decreased from 6.8 (before) to 3.6 (after), indicating that protons are released into the aqueous phase. This suggests that firstly, there is the transfer of HSO<sub>4</sub><sup>-</sup> to the aqueous phase and then there is the dissociation of the HSO<sub>4</sub><sup>-</sup> to SO<sub>4</sub><sup>2-</sup>. The transfer of HSO<sub>4</sub><sup>-</sup> to the aqueous phase is driven by the hydration energy of sulfate (1080 kJ mol<sup>-1</sup>),<sup>46</sup> formed upon dissociation of hydrogen sulfate to sulfate and protons. Evidence of this transfer was supported by Raman spectroscopy (see Figs. S2 and S3).



**Figure 3.** Raman spectra for BaSO<sub>4</sub> crystallisation at the ITIES: (A) formed between organic solution of Ba(TPBCl)<sub>2</sub> and aqueous solution of SO<sub>4</sub><sup>2-</sup> (Scheme 1); (B) formed between aqueous solution of Ba<sup>2+</sup> ions and organic solution of TBuAHSO<sub>4</sub> (Scheme 2). KTPBCl is potassium tetrakis(4-chlorophenyl)borate. TBuAHSO<sub>4</sub> is tetrabutylammonium hydrogensulfate. Reference indicates the spectrum of commercially-available material.

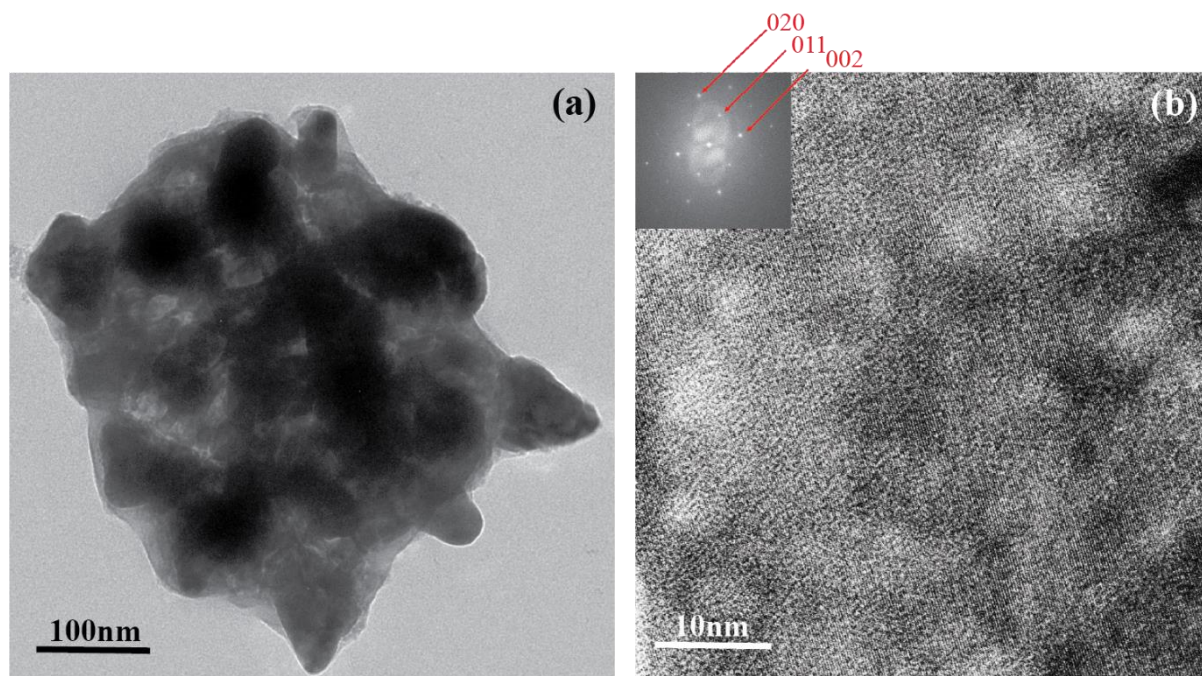
SEM in combination with EDS was used to examine the morphological and qualitative characteristics of the BaSO<sub>4</sub> products. Crystallisation occurred when Ba<sup>2+</sup> ions were placed in either the organic phase (Fig. 4, A) or the aqueous phase (Fig. 4, B) with the corresponding co-reactant in the adjoining phase as either SO<sub>4</sub><sup>2-</sup> or HSO<sub>4</sub><sup>-</sup>, respectively. The SEM images clearly reveal that new solid particles precipitated at or close to the micro-interfaces. EDS single point spectra were acquired from both products (Fig. 4 A&B) at two different positions. According to the EDS data position ‘a’ (Fig. 4), BaSO<sub>4</sub> crystallisation occurred with Ba<sup>2+</sup> placed in the organic phase (Ba(TPBCl)<sub>2</sub> in DCE) in contact with an aqueous solution of Na<sub>2</sub>SO<sub>4</sub>. A finding of Si with no signs of Ba or S in the matrix region (Fig. 4, position ‘b’) indicates that BaSO<sub>4</sub> has not precipitated far away from the glass membrane micropores. Position ‘c’ (Fig. 4) shows a large area of precipitation on the membrane where the interface between the aqueous solution containing Ba<sup>2+</sup> ions and organic solution of HSO<sub>4</sub><sup>-</sup> was formed (Fig. 4, image B). The EDS spectrum of position ‘c’ (large area) confirms the presence of Ba, S, and O and their co-location clearly supports that BaSO<sub>4</sub> was formed. The spectrum of position ‘d’ shows there is no BaSO<sub>4</sub> in this area; the Si signal results from the glass membrane. Additionally, EDS line scans across the crystalline materials on the glass microporous membranes were performed to study

elemental distribution (Figure S4(a, b) for electrochemical cell Scheme 1 and Figure S4(c, d) for Scheme 2). Figure S4(b, d) show the presence of Ba, S and O together where BaSO<sub>4</sub> crystals formed on the glass membranes.



**Figure 4.** SEM and EDS analysis of barium sulfate solids precipitated at liquid-liquid interfaces supported on a glass microporous membrane. (A) SEM micrograph of BaSO<sub>4</sub> crystal deposited between an aqueous solution containing sulfate ions and an organic solution containing barium ions (Scheme 1) and EDS spectra for positions 'a' and 'b' shown in the SEM. (B) SEM micrograph of BaSO<sub>4</sub> crystal deposited between an aqueous solution containing BaCl<sub>2</sub> and an organic solution containing TBuAHSO<sub>4</sub> (Scheme 2) and EDS spectra at position 'c' and 'd' shown in the SEM

Further analysis of the particles formed at or close to the interface was undertaken using TEM, to determine the morphology of the particles and confirm their elemental compositions. The precipitated particles formed at the micro-interfaces were removed from the glass membrane surface by sonication and transferred to a TEM grid. Fig. 5a presents the TEM images of BaSO<sub>4</sub> precipitated at the interface between 0.5 mM Ba(TPBCl)<sub>2</sub> (plus 10 mM BTPPATPBCl) organic phase and 10 mM Na<sub>2</sub>SO<sub>4</sub> aqueous phase (Scheme 1). The morphology shown in this figure is irregular in shape and appears to be composed of smaller particles. Crystallinity was confirmed by HRTEM and Fast Fourier Transform (FFT) patterns which displayed clear spots that were assigned to Miller planes of barium sulfate (inset, Fig. 5b). BaSO<sub>4</sub> crystallisation also occurred at the interface between 10 mM aqueous BaCl<sub>2</sub> and 0.1 M TBuAHSO<sub>4</sub> organic phase (Scheme 2). From the TEM images of crystalline BaSO<sub>4</sub> (Figure 5c) it can be seen that the morphology is also irregular and consists of smaller particles. Crystallinity was confirmed by HRTEM and FFT patterns were assigned to Miller planes of barium sulfate (inset, Fig. 5d). In addition, the lack of rings in the FFT patterns means that, at least in the area the FFTs were taken, the smaller particles were aligned. Crystallisation of barium sulfate at the ITIES by spontaneous transfer of either reactant from organic to aqueous phase was also confirmed by HAADF-TEM images with corresponding elemental particle maps (Figures S5 and S6). The homogeneous distributions of Ba and S in these maps indicates the formation of ionic crystalline materials.





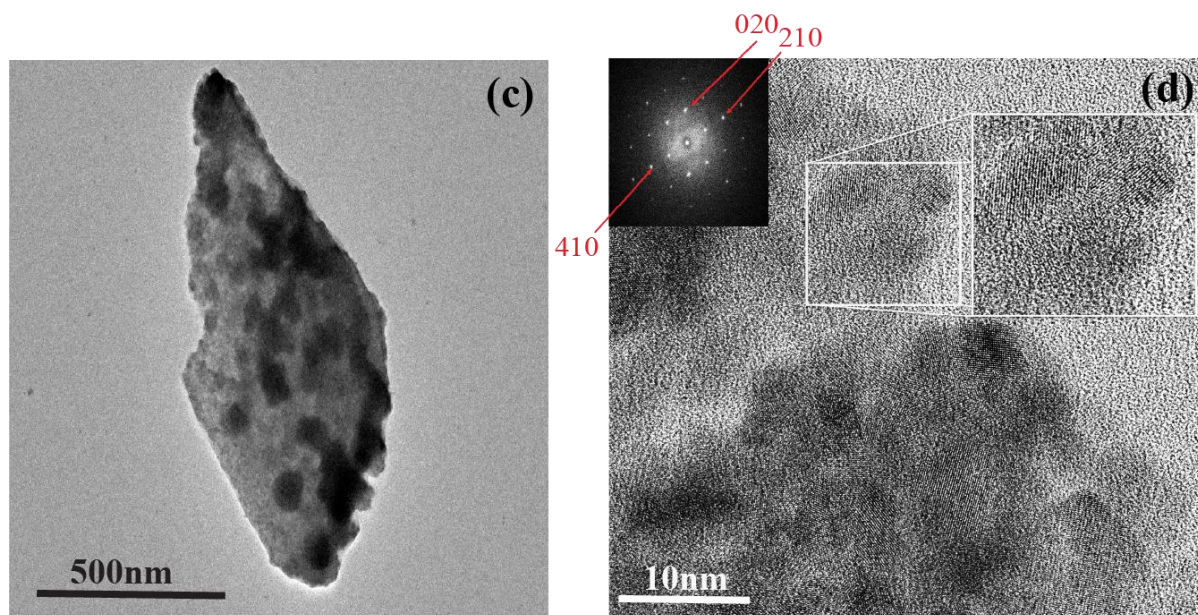


**Figure 5.** Representative TEM and HRTEM images and corresponding FFT patterns of BaSO<sub>4</sub> formed at the interface of Ba<sup>2+</sup> in the organic phase and SO<sub>4</sub><sup>2-</sup> in the aqueous phase (a,b) or Ba<sup>2+</sup> in the aqueous solution and HSO<sub>4</sub><sup>-</sup> in the organic phase (c,d).

### 3.3. Impact of ionophore as an organic phase dopant

The impact of organic-phase ionophore on the crystallisation of barium sulfate was investigated. By addition of a suitable ionophore to the organic phase containing Ba<sup>2+</sup> cations, it was anticipated that the Ba<sup>2+</sup> would be stabilised in the organic phase and show less tendency to transfer to a contacting aqueous phase – the net result would be less or no crystallisation. When such an experiment was undertaken in the glass capillary set-up, no precipitate was observed. Likewise, the Raman spectra recorded at the capillary mouth (Fig. 6) show that in the presence of organic phase Calcium Ionophore IV (1 mM), BaSO<sub>4</sub> formation was not detected at the interface located at the mouth of a glass capillary. In this case, the ionophore complexed the Ba<sup>2+</sup> cations in the organic phase, which is consistent with selectivity data for calcium ion-selective electrodes<sup>38</sup> using this ionophore, which show that Ba<sup>2+</sup> cations are complexed by this neutral ionophore. Hence, the presence of the ionophore inhibited spontaneous ion transfer from the organic phase to the aqueous phase, i.e. stabilising the cation in the organic phase, and hence no precipitation was observed. This observation confirms that ions from the organic phase transfer across the interface to react on the aqueous side of the interface, and not vice versa. As the role of ionophores are to enable stability of ions within less polar phases than water, they achieve this by altering the solvation in that less polar phase. In this case, with ionophore Calcium Ionophore IV, it complexes Ba<sup>2+</sup> cations and shields them from the solvent, i.e. the complex is solvated rather than the inorganic ion. This improves the stability of barium within the organic phase and

renders it less likely to be driven to the aqueous phase by its hydration energy. In effect the concentration of the available  $\text{Ba}^{2+}$  ions are minimised, so that no resultant precipitation of  $\text{BaSO}_4$  is seen. Ultimately, the presence of ionophore suggests an approach to control the crystallisation of barium sulfate at the ITIES.

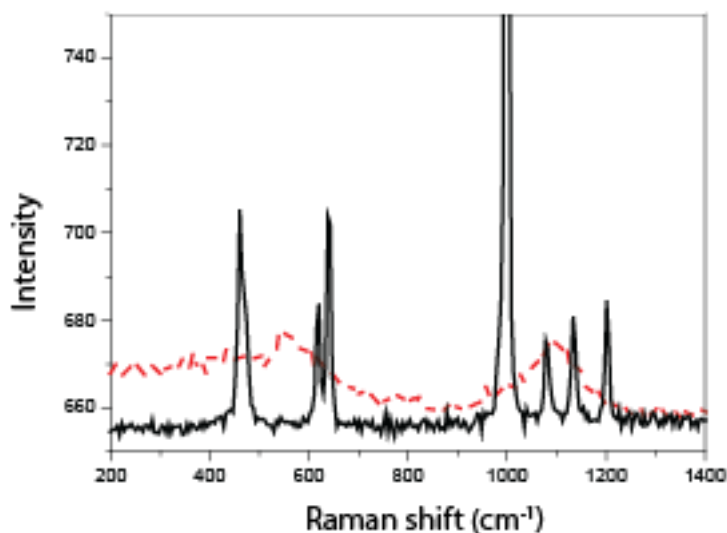


**Figure 6.** Raman spectra for  $\text{BaSO}_4$  crystallisation, in the absence of organic phase ionophore (solid line) and in the presence of organic phase ionophore (dashed line), indicating no formation of  $\text{BaSO}_4$  in the latter. Raman spectra were taken from the mouth of the capillary in each case.

In order to assess the action of the ionophore, preliminary open-circuit potential (OCP) measurements of the cells depicted in Schemes 1 and 2 were performed. The OCP was measured in cases where barium ions were placed in either the organic (Fig.7A) or aqueous phases (Fig.7B) and the co-reactant sulfate in the adjoining phase, respectively. After 4000 s, the potential difference between the organic solution containing 0.5 mM  $\text{Ba}(\text{TPBCl})_2$  and 10 mM  $\text{BTPPATPBCl}$  in DCE and aqueous solution of 10 mM  $\text{Na}_2\text{SO}_4$  (Scheme 1) was about -0.1 V, while between the aqueous solution of 10 mM  $\text{BaCl}_2$  and organic solution of 0.1 M  $\text{TBuAHSO}_4$  (Scheme 2) this value was ca. 0.03 V. From Fig.7C it can be found that the potential difference between the two immiscible solutions was -0.1 V in the presence of 1 mM calcium ionophore IV with  $\text{Ba}^{2+}$  in the organic phase, however, a stable value was not reached within the duration studied (4000 s). More importantly, the trends in OCP with time indicate changes occurring within the cell during the course of the experiments. Fig. 7A shows a high initial potential, consistent with  $\text{Ba}^{2+}$  transfer from the organic to the aqueous phase. This high potential drops gradually in the initial period, before suddenly dropping to a stable value of ca. -0.1 V. This may indicate the

gradual formation of precipitate at the interfaces which blocks the pores so that no further ion transfer occurs. In contrast, in the presence of ionophore (Fig. 7C), the initial potential is positive but not as high as in the absence of ionophore, which is consistent with transfer of less  $\text{Ba}^{2+}$  cations to the aqueous phase. In this situation, there is a continued steady decline in the OCP with time, indicating that some changes occur, perhaps transfer of very small amounts of  $\text{Ba}^{2+}$  to the aqueous phase, but no blockage of the interface occurs as there is no sudden drop in OCP. Blockage and no blockage of the interfaces in these experiments is supported by subsequent SEM imaging of the glass membranes. The images in Figure 7(a, b) show that crystals were formed when either organic or aqueous solutions containing barium ion were present, but no  $\text{BaSO}_4$  crystallisation was seen in the presence of ionophore (Fig. 7c). From EDS data, only Si, O and Na were found on the microporous membrane when ionophore was present.

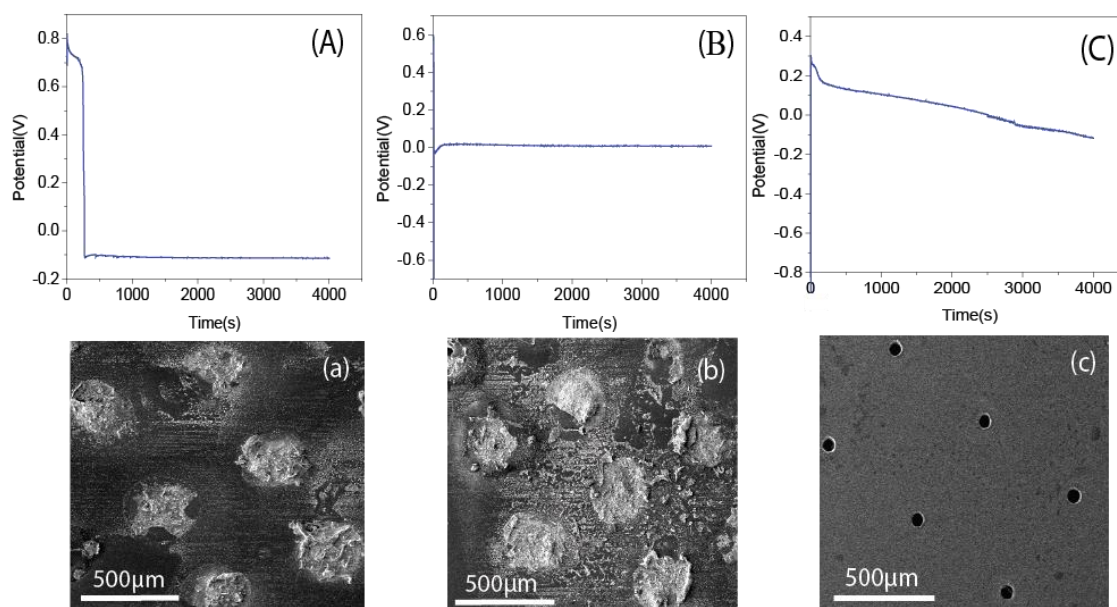


Figure 7. Open-circuit potential measurements of barium sulfate formation at liquid-liquid interfaces located at glass microporous membranes. (A) Sulfate ions in the aqueous phase and barium ions in the organic phase (Scheme 1). (B) Sulfate ions in the organic phase, as hydrogen sulfate, and barium ions in the aqueous phase. (C) Organic solution containing barium ions with Calcium Ionophore IV (1 mM) present and an aqueous phase of sulfate solution. (a) and (b) SEM images show barium sulfate precipitated in absence of ionophore according to (A) and (B) conditions, respectively. (c) SEM shows no barium sulfate precipitation in presence of Calcium Ionophore IV, based on (C).

#### 4. Conclusion

Interfacial formation of crystalline  $\text{BaSO}_4$  occurred upon ion transfer across the interface between two immiscible electrolyte solutions. Transfer of  $\text{Ba}^{2+}$  ions from the organic phase to the aqueous phase

containing  $\text{SO}_4^{2-}$  lead to barium sulfate crystallisation at the interface in both glass capillary and microporous membrane array experiments. Raman spectroscopy confirmed that the collected product at the interface was barium sulfate. Spontaneous ion transfer and interfacial formation of  $\text{BaSO}_4$  were also investigated with aqueous solutions of  $\text{BaCl}_2$  and an organic phase containing  $\text{TBuAHSO}_4$ . Based on Raman spectroscopy, SEM-EDS and TEM, it is clearly seen that liquid-liquid interfacial barium sulfate crystallisation occurred upon spontaneous ion transfer from the organic phase to the aqueous phase.

The spontaneous transfer of barium ions across organic/aqueous interface coupled with subsequent crystal formation was inhibited by the presence of an ionophore in the organic phase. This ionophore stabilises barium cations in the organic phase, decreasing their drive to transfer to the adjoining water phase. Based on Raman spectroscopy, it was clearly observed that contact of the organic phase containing  $\text{Ba}^{2+}$  with the aqueous phase of sodium sulfate did not result in the spontaneous formation of barium sulfate when calcium ionophore IV was present in the organic solution. Accordingly, these results provide a basis to control the spontaneous transfer and crystallisation at liquid-liquid interfaces by addition of suitable ion-binding materials.

### Conflicts of Interest

There are no conflicts of interest to declare.

### Acknowledgements

NG is supported by a research scholarship from Curtin University and BBJA by an Australian Government Research Training Program Scholarship and the Rowe Scientific Scholarship. GH thanks the CNRS for financial support through its International Emerging Actions scheme (Project Elixir). The authors are grateful to Jiayi Chen for taking the TEM measurements. The authors acknowledge the use of equipment, scientific, and technical assistance of the John de Laeter Centre, Curtin University, funded by the University and by the State and Commonwealth Governments. The authors acknowledge the facilities, and the scientific and technical assistance of Microscopy Australia at the Centre for Microscopy, Characterisation & Analysis, University of Western Australia, a facility funded by the University, and the State and Commonwealth Governments. The authors gratefully acknowledge the South Australian and OptoFab nodes of the NCRIS-enabled Australian National Fabrication Facility (ANFF-SA and ANFFOptoFab, respectively) for preparation of the glass microporous membranes.

### References

1. Kirwan, D.; Orella, C., Crystallization in the pharmaceutical and bioprocessing industries. In *Handbook of industrial crystallization*, Elsevier: 2002; pp 249-266.
2. Ma, Y.; Wu, S.; Macaringue, E. G. J.; Zhang, T.; Gong, J.; Wang, J., Recent progress in continuous crystallization of pharmaceutical products: precise preparation and control. *Organic Process Research & Development* **2020**, *24* (10), 1785-1801.
3. Blagden, N.; de Matas, M.; Gavan, P. T.; York, P., Crystal engineering of active pharmaceutical ingredients to improve solubility and dissolution rates. *Advanced drug delivery reviews* **2007**, *59* (7), 617-630.



4. Pramanik, B. K.; Thangavadivel, K.; Shu, L.; Jegatheesan, V., A critical review of membrane crystallization for the purification of water and recovery of minerals. *Reviews in Environmental Science and Bio/Technology* **2016**, *15* (3), 411-439.
5. Frenier, W. W.; Ziauddin, M., *Formation, removal, and inhibition of inorganic scale in the oilfield environment*. Society of Petroleum Engineers Richardson, TX: 2008.
6. Al Kalbani, M.; Jordan, M.; Mackay, E.; Sorbie, K.; Nghiem, L., Barium Sulfate Scaling and Control during Polymer, Surfactant, and Surfactant/Polymer Flooding. *SPE Production & Operations* **2020**, *35* (01), 068-084.
7. Hirsch, R. E.; Raventos-Suarez, C.; Olson, J. A.; Nagel, R. L., Ligand state of intraerythrocytic circulating HbC crystals in homozygote CC patients. *Blood* **1985**, *66* (4), 775-777.
8. Ferrone, F. A.; Hofrichter, J.; Eaton, W. A., Kinetics of sickle hemoglobin polymerization: II. A double nucleation mechanism. *Journal of molecular biology* **1985**, *183* (4), 611-631.
9. Berland, C. R.; Thurston, G. M.; Kondo, M.; Broide, M. L.; Pande, J.; Ogun, O.; Benedek, G. B., Solid-liquid phase boundaries of lens protein solutions. *Proceedings of the National Academy of Sciences* **1992**, *89* (4), 1214-1218.
10. Antonious, M. S., Effect of additives on the crystallization of barium sulphate. *Phosphorus, Sulfur, and Silicon and the Related Elements* **1996**, *112* (1-4), 235-245.
11. Hausler, R., Predicting and controlling scale from oil-field brines. *OIL & GAS JOURNAL* **1978**, *76* (38), 146-&.
12. Quddus, A.; Allam, I., BaSO<sub>4</sub> scale deposition on stainless steel. *Desalination* **2000**, *127* (3), 219-224.
13. Sorbie, K. S.; Laing, N. In *How scale inhibitors work: Mechanisms of selected barium sulphate scale inhibitors across a wide temperature range*, SPE International Symposium on Oilfield Scale, OnePetro: 2004.
14. Athanasopoulos, E. D.; Armakola, E.; Koutsoukos, P. G.; Demadis, K. D., Nucleation and crystal growth of barium sulfate: inhibition in the presence of rigid and flexible triphosphonate additives. *CrystEngComm* **2018**, *20* (41), 6589-6601.
15. Allison, S. K., The reflection of X-rays by barite. *American Journal of Science* **1924**, *5* (46), 261-276.
16. James, R. W.; Wood, W., The crystal structure of barytes, celestine and anglesite. *Proceedings of the Royal Society of London. Series A, Containing Papers of a Mathematical and Physical Character* **1925**, *109* (752), 598-620.
17. Jellinek, F., On barium manganate and some related compounds. *Journal of Inorganic and Nuclear Chemistry* **1960**, *13* (3-4), 329-331.
18. Kou, Y.; Wang, Y.; Zhang, J.; Guo, K.; Zhang, X.; Yu, Z.; Song, X., Nano BaSO<sub>4</sub> prepared by microreactor and its effect on thermal decomposition of some energetics. *FirePhysChem* **2021**.
19. Ruiz-Agudo, C.; Ruiz-Agudo, E.; Putnis, C. V.; Putnis, A., Mechanistic principles of barite formation: from nanoparticles to micron-sized crystals. *Crystal Growth & Design* **2015**, *15* (8), 3724-3733.
20. Weber, J.; Barthel, J.; Brandt, F.; Klinkenberg, M.; Breuer, U.; Kruth, M.; Bosbach, D., Nano-structural features of barite crystals observed by electron microscopy and atom probe tomography. *Chemical geology* **2016**, *424*, 51-59.
21. Jones, F.; Oliveira, A.; Rohl, A.; Parkinson, G.; Ogden, M.; Reyhani, M., Investigation into the effect of phosphonate inhibitors on barium sulfate precipitation. *Journal of Crystal Growth* **2002**, *237*, 424-429.
22. Kelland, M. A., Effect of various cations on the formation of calcium carbonate and barium sulfate scale with and without scale inhibitors. *Industrial & Engineering Chemistry Research* **2011**, *50* (9), 5852-5861.
23. Leng, H.; Wang, X.; Ross, R. D.; Niebur, G. L.; Roeder, R. K., Micro-computed tomography of fatigue microdamage in cortical bone using a barium sulfate contrast agent. *Journal of the mechanical behavior of biomedical materials* **2008**, *1* (1), 68-75.
24. Liu, J.-W.; Guo, X.-Q.; Tian, M.-W.; Qu, L.-J.; Yu, N., Preparation and Radiation Protection Property of Nano Barium Sulfate/Cellulose Composite Membrane. *Journal of Qingdao University(Engineering & Technology edition)* **2013**, *28* (1).
25. Merdhah, A. B. B.; Yassin, A. A. M., Barium sulfate scale formation in oil reservoir during water injection at high-barium formation water. *J. Appl. Sci* **2007**, *7* (17), 2393-2403.

26. Sosso, G. C.; Chen, J.; Cox, S. J.; Fitzner, M.; Pedevilla, P.; Zen, A.; Michaelides, A., Crystal nucleation in liquids: Open questions and future challenges in molecular dynamics simulations. *Chemical reviews* **2016**, *116* (12), 7078-7116.
27. Weber, J.; Bracco, J. N.; Yuan, K.; Starchenko, V.; Stack, A. G., Studies of Mineral Nucleation and Growth Across Multiple Scales: Review of the Current State of Research Using the Example of Barite (BaSO<sub>4</sub>). *ACS Earth and Space Chemistry* **2021**, *5* (12), 3338-3361.
28. Dai, C.; Stack, A. G.; Koishi, A.; Fernandez-Martinez, A.; Lee, S. S.; Hu, Y., Heterogeneous nucleation and growth of barium sulfate at organic–water interfaces: interplay between surface hydrophobicity and Ba<sup>2+</sup> adsorption. *Langmuir* **2016**, *32* (21), 5277-5284.
29. Aizenberg, J.; Black, A. J.; Whitesides, G. M., Control of crystal nucleation by patterned self-assembled monolayers. *Nature* **1999**, *398* (6727), 495-498.
30. Ray, D. R.; Kumar, A.; Reddy, S.; Sainkar, S.; Pavaskar, N.; Sastry, M., Morphology of BaSO<sub>4</sub> crystals grown at the liquid–liquid interface. *CrystEngComm* **2001**, *3* (45), 213-216.
31. Rautaray, D.; Banpurkar, A.; Sainkar, S. R.; Limaye, A. V.; Ogale, S.; Sastry, M., BaSO<sub>4</sub> Crystals Grown at an Expanding Liquid–Liquid Interface in a Radial Hele-Shaw Cell Show Spontaneous Large-Scale Assembly into Filaments. *Crystal growth & design* **2003**, *3* (4), 449-452.
32. Matsuoka, R.; Sakamoto, R.; Hoshiko, K.; Sasaki, S.; Masunaga, H.; Nagashio, K.; Nishihara, H., Crystalline graphdiyne nanosheets produced at a gas/liquid or liquid/liquid interface. *Journal of the American Chemical Society* **2017**, *139* (8), 3145-3152.
33. Tatsukawa, S.; Kadota, K.; Yoshida, M.; Shirakawa, Y., Development of quantifying supersaturation to determine the effect of the anti-solvent on precipitation in liquid-liquid interfacial crystallization. *Journal of Molecular Liquids* **2020**, *309*, 113097.
34. Ravenhill, E. R.; Kirkman, P. M.; Unwin, P. R., Microscopic Studies of Calcium Sulfate Crystallization and Transformation at Aqueous–Organic Interfaces. *Crystal Growth & Design* **2016**, *16* (10), 5887-5895.
35. Girault, H. H., Electrochemistry at liquid–liquid interfaces. *Electroanalytical chemistry* **2010**, *23*, 1-104.
36. Kaliszczak, M.; Durand, P.; Wenger, E.; Dossot, M.; Jones, F.; Arrigan, D. W.; Herzog, G., Electrochemically controlled cocrystallisation of caffeine: 1-hydroxy-2-naphthoic acid. *CrystEngComm* **2022**, *24* (1), 48-51.
37. Bühlmann, P.; Pretsch, E.; Bakker, E., Carrier-based ion-selective electrodes and bulk optodes. 2. Ionophores for potentiometric and optical sensors. *Chemical Reviews* **1998**, *98* (4), 1593-1688.
38. Ishimatsu, R.; Izadyar, A.; Kabagambe, B.; Kim, Y.; Kim, J.; Amemiya, S., Electrochemical mechanism of ion–ionophore recognition at plasticized polymer membrane/water interfaces. *Journal of the American Chemical Society* **2011**, *133* (40), 16300-16308.
39. Piradashvili, K.; Alexandrino, E. M.; Wurm, F. R.; Landfester, K., Reactions and polymerizations at the liquid–liquid interface. *Chemical reviews* **2016**, *116* (4), 2141-2169.
40. He, L.; Dexter, A. F.; Middelberg, A. P., Biomolecular engineering at interfaces. *Chemical engineering science* **2006**, *61* (3), 989-1003.
41. Ji, T.; Liang, Z.; Zhu, X.; Wang, L.; Liu, S.; Shao, Y., Probing the structure of a water/nitrobenzene interface by scanning ion conductance microscopy. *Chemical Science* **2011**, *2* (8), 1523-1529.
42. Beattie, P.; Delay, A.; Girault, H., Investigation of the kinetics of assisted potassium ion transfer by dibenzo-18-crown-6 at the micro-ITIES by means of steady-state voltammetry. *Journal of Electroanalytical Chemistry* **1995**, *380* (1-2), 167-175.
43. Uyanik, M.; Nakashima, D.; Ishihara, K., Baeyer–Villiger oxidation and oxidative cascade reactions with aqueous hydrogen peroxide catalyzed by lipophilic Li [B (C<sub>6</sub>F<sub>5</sub>)<sub>4</sub>] and Ca [B (C<sub>6</sub>F<sub>5</sub>)<sub>4</sub>]<sub>2</sub>. *Angewandte Chemie* **2012**, *124* (36), 9227-9230.
44. de Eulate, E. A.; Strutwolf, J.; Liu, Y.; O'Donnell, K.; Arrigan, D. W., An electrochemical sensing platform based on liquid-liquid microinterface arrays formed in laser-ablated glass membranes. *Analytical chemistry* **2016**, *88* (5), 2596-2604.

45. Alvarez de Eulate, E.; Arrigan, D. W., Adsorptive stripping voltammetry of hen-egg-white-lysozyme via adsorption–desorption at an array of liquid–liquid microinterfaces. *Analytical chemistry* **2012**, *84* (5), 2505-2511.
46. Smith, D. W., Ionic hydration enthalpies. *Journal of Chemical Education* **1977**, *54* (9), 540.
47. McKeown, D. A.; Muller, I. S.; Gan, H.; Pegg, I. L.; Kendziora, C. A., Raman studies of sulfur in borosilicate waste glasses: sulfate environments. *Journal of Non-Crystalline Solids* **2001**, *288* (1-3), 191-199.
48. Adler, H. H.; Kerr, P. F., Variations in infrared spectra, molecular symmetry and site symmetry of sulfate minerals. *American Mineralogist: Journal of Earth and Planetary Materials* **1965**, *50* (1-2), 132-147.
49. Wylde, J. J.; Allen, G. C.; Collins, I. R., FT-IR and Raman spectroscopic characterization of the major oilfield sulfate scale forming minerals. *Applied Spectroscopy* **2001**, *55* (9), 1155-1160.
50. Ferguson, R. J.; Ferguson, B. R., The chemistry of strontium and barium scales. *Association of Water Technologies* **2010**, 1-17.